The Scaling of Secondary Craters. S. K. Croft, Lunar & Planetary Laboratory, University of Arizona, Tucson, AZ, 85721.

Secondary craters are common features around fresh planetary-scale primary impact craters throughout most of the Solar System. They derive from the ejection phase of crater formation, thus secondary scaling relations provide constraints on parameters affecting ejection processes. Secondary crater fields typically begin at the edge of the continuous ejecta blanket (CEB) and extend out several crater radii. Secondaries occur singly and in groups: clusters, radial chains and loops. Individual secondaries tend to have rounded rims and bilateral symmetry about an axis through the primary crater's center. Prominent secondary chains (e.g., Vallis Bouvard/Baade south of Orientale Basin on the Moon) can extend inward across the continuous ejecta blanket close to the rim. Such chains are more common on Mercury than on other planets.

A simple method for comparing secondary crater fields was employed by Allen (ref. 1): averaging the diameters and ranges from the center of the primary crater of the five largest craters in a secondary crater field. While not as much information is obtained about individual crater fields by this method as in more complete secondary field mappings (2,3,4), Allen's method facilitates rapid comparison of many secondary fields. Also, by quantifying a few specific aspects of the secondary crater field, Allen's method can be used to construct scaling relations for secondary craters, something which has not been done in the more detailed studies.

The diameters of the largest secondaries (D_s) around primaries on the Moon (1), Ganymede (5), Mercury, and Mars are shown as functions of the primary crater rim diameter (D_r) in fig. 1. The functional dependence of D_s on D_r is remarkably consistent on all four planets: $D_s \approx 0.07\ D_r^{0.87}$. The mean ranges of the largest secondaries (R_s) on all four planets are also very similar and can be represented by: $R_s \approx 3\ D_r^{0.86}$. (Complete numerical analyses are given in ref. 6). These empirical results may be quantitatively interpreted. The ejecta scaling theory of (7) indicates that the ballistic range of bits of ejecta scale with the diameter (D_p) of the gravity-scaled primary crater: $R_s \propto D_p^{1}$. Virtually all of the craters in the sample are complex, thus the empirical relation (8) between the gravity-scaled transient crater rim and the slump-enlarged final crater rim ($D_p \propto D_r^{0.85\pm0.05}$) can be applied, yielding: $R_s \propto D_r^{0.85\pm0.05}$, in agreement with the observed relation. Similarly, combining the crater-scaling relation of (8) with the ballistic equation and the secondary range relation yields: $D_s \propto D_p^{B}\ a_s^{1-B}$, where B is the radius-scaling exponent of (8), and D_s and a_s are, respectively, the secondary crater rim diameter and secondary impactor radius. Various assumptions can be made concerning the scaling of a_s to transform the above relation into a form comparable with observation. Adopting the spall model of (9), a model frequently invoked to account for secondary impactors, yields: $D_s \propto D_p^{1-(n-1)B}$, where n is the velocity exponent in the relation between ejection velocity and distance from point of impact. Inserting the probable values of n between 2 and 3, B = 0.17 (8), and complex rim diameter yields: $D_s \propto D_r^{0.56 \text{ to } 0.71}$. This is inconsistent with observation, indicating that the secondary impactors are not spalls. This result is consistent with the computational and experimental results of (10), who were also unable to confirm the spall model. Alternatively, assuming $a_s \propto a_p$, the primary impactor radius, yields: $D_s \propto D_p^{1+B}$, or $D_s \propto D_r^{0.99}$, again inconsistent with observation. An assumption that works is: $a_s \propto D_p$, which yields $D_s \propto D_p^{1}$, or $D_s \propto D_r^{0.85}$ for complex craters. Empirical ejecta scaling relations developed in (6) imply that the ejecta curtain fragments at a thickness that also scales with D_p to form the edge of the CEB. The correspondence in scaling and geometry between the CEB edge and secondary impactor radii suggests that both originate in the same fragmentation process in the cratering flow field.

Secondary crater fields are seldom seen on the smaller icy satellites. Secondary crater chains have been proposed for Arden on Miranda (11) and possibly for Odysseus on Tethys (6, prompted by the maps of 12), against which two objections have been raised: 1) fragments forming secondary craters move much too fast to be retained on any middle-sized icy satellite (13), and 2) large secondary craters cannot form from very slow moving (<100 m/s) ejecta because of the low cratering efficiencies (ratio of crater volume to impactor volume) near unity; secondary mounds are the more likely outcome (14). The first objection is based on the assumption that the secondary impactors are the spalls of (9), an assumption indicated as incorrect by these results. But in either case, the computed impact velocities of impactors forming undisputed secondaries on the terrestrial planets are not absolute, relating, for example, to the primary impactor velocity, but scale with the primary crater diameter (as required by ejecta scaling theory (7)), reaching as low as 50 m/s in Allen's lunar data set (1). As long as gravity scaling applies, primary craters on smaller icy satellites should eject secondary-forming fragments at velocities low enough to be retained and form secondary craters. The validity of the second objection was tested by measuring the diameters and ranges of craters in prominent radial chains on the Moon, Mercury, and Ganymede, and the proposed chains on Miranda, and computing the cratering efficiencies (PI-V) using the scaling of (8). The resulting PI-V's are shown as functions of normalized range in Fig. 2. As may be seen, the cratering efficiencies of all large secondaries are near unity, but recognizable secondary craters are formed nonetheless. Thus the suggestion that secondary mounds would form for PI-V's near unity is not supported by

the data. The proposed Arden chains show the same absolute PI-V's and radial trends as the recognized secondary chains to which they were first compared (5). This result is consistent with the explicit cancellation of gravity out of ejecta scaling (7) and the secondary crater scaling relations derived above, which implies that, as long as gravity scaling applies, secondaries should form on arbitrarily small moons. Thus the Arden chains cannot be rejected as secondaries by scaling arguments. Similarly, secondary crater fields should be observed on smaller icy satellites. Where are they? A compilation given in (6) comparing secondary crater diameters predicted from the empirical relation in Fig 1 with resolutions in the best Voyager images of the smaller icy satellites indicates that, in most cases, the secondaries are at or below the limit of resolution. In those few cases where the predicted secondaries should be seen, they either are seen, or are found on surfaces too heavily cratered to confidently identify secondaries. Thus it is proposed that secondaries do occur on all icy satellites where gravity scaling applies, a proposal that will be tested by the Cassini spacecraft.

References. 1)Allen (1979) GRL 6:51. 2) Gault et al. (1975) JGR 80:2444. 3) Schultz & Singer (1980) PLPSC 11th, p. 2243. 4) Vickery (1986) Icarus 67:224. 5) Croft (1988) LPS XIX, p. 221. 6) Croft (1991), Icarus, submitted. 7) Housen et al (1983) JGR 88:2485. 8) Schmidt & Housen (1987) Int J Imp Eng 5:543. 9) Melosh (1984) Icarus 59:234. 10) Holsapple, K.A. & K.Y. Choe (1988) LPS XIX, p. 501-502. 11) Croft (1987) NASA TM 89810, p. 6. 12) Moore & Ahern (1983) PLPSC 13th, JGR 88(supp):A577. 13) Chapman & McKinnon (1986) Satellites, p. 492, U. of Ariz Press. 14) McKinnon & Chapman (1990) Uranus, in press, U of Ariz Press.

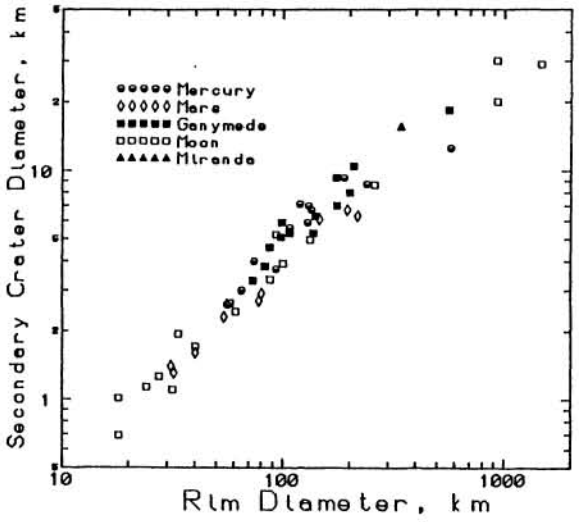

Figure 1. Mean Largest Secondary Crater Diameter vs. Primary Crater Rim Diameter.

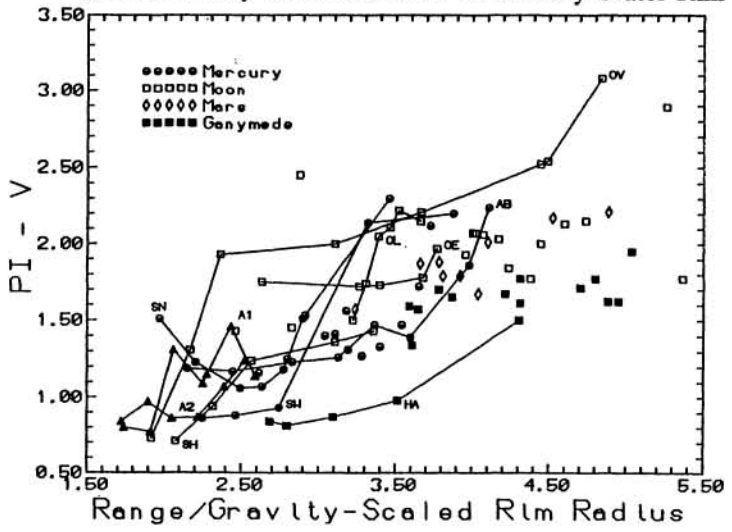

Figure 2. Cratering Efficiency (PI-V) vs. Normalized Range for Largest Secondaries in Fig. 1 and Selected Radial Crater Chains (connected symbols): OE,OL, and OV = Orientale (Moon); SH = Schrodinger (Moon); SW, SN = Strindberg (Mercury); AB = Ahmed Baba (Mercury); HA = Halieus (Ganymede); A1, A2 = Arden (Miranda).